electronics

MDPI

Article

Study on Thermal Characteristics of Winding under Inter-Turn Fault of Oil-Immersed Transformer

Yuefeng Hao [1], Zhanlong Zhang [1,*], Jiayi Xiao [1,2], Hui Zhao [1,3], Yu Yang [1] and Zijian Dong [1]

[1] School of Electrical Engineering, Chongqing University, Chongqing 400044, China; 20201101076g@stu.cqu.edu.cn (Y.H.); 202111021026@cqu.edu.cn (J.X.); 20191101372@stu.cqu.edu.cn (H.Z.); 20163724@cqu.edu.cn (Y.Y.); dongzi@cqu.edu.cn (Z.D.)
[2] State Grid Hunan Extra High Voltage Substation Company, Changsha 410005, China
[3] Central Southern China Electric Power Design Institute, Wuhan 430071, China
* Correspondence: zhangzl@cqu.edu.cn

Abstract: The inter-turn fault is a common fault of oil-immersed transformers. Due to the deterioration of inter-turn insulation, its resistance decreases, which leads to an increase in the winding coil current and loss, causing the winding temperature to rise. Therefore, analyzing the electrothermal characteristics of inter-turn short circuit faults in oil-immersed transformers can provide a theoretical basis for the diagnosis of inter-turn faults in transformers. This paper studies the equivalent circuit under inter-turn faults and establishes a field–circuit coupling model to calculate the current characteristics under different inter-turn short circuit faults of transformers. The distribution of coil losses under faults is calculated as thermal source excitations, and a thermal–fluid-coupled calculation model for oil-immersed transformers is established. After the experimental verification, it is found that both the errors between the winding and tank surface temperatures do not exceed the acceptable limits, validating the effectiveness of this model. Using this model to calculate the temperature distribution for various inter-turn short circuit faults in transformers reveals their hot-spot characteristics. The results indicate that under inter-turn fault conditions, the temperature at faulty turns will gradually increase towards a limit, eventually leading to coil damage. This research provides theoretical support for enhancing transformer detection and diagnostic capabilities.

Keywords: oil-immersed transformer; inter-turn fault of winding; thermal–fluid coupling

check for updates

Citation: Hao, Y.; Zhang, Z.; Xiao, J.; Zhao, H.; Yang, Y.; Dong, Z. Study on Thermal Characteristics of Winding under Inter-Turn Fault of Oil-Immersed Transformer. *Electronics* **2024**, *13*, 2869. https://doi.org/10.3390/electronics13142869

Academic Editor: Ahmed Abu-Siada

Received: 18 June 2024
Revised: 12 July 2024
Accepted: 15 July 2024
Published: 21 July 2024

Copyright: © 2024 by the authors. Licensee MDPI, Basel, Switzerland. This article is an open access article distributed under the terms and conditions of the Creative Commons Attribution (CC BY) license (https://creativecommons.org/licenses/by/4.0/).

1. Introduction

The oil-immersed power transformer is crucial for ensuring the reliable and stable operation of the power system, characterized by its wide distribution and large number [1]. The service life of a transformer depends on the degree of the aging of oil–paper insulation, with thermal aging being the main factor leading to oil–paper insulation aging. The increase in the internal temperature of the transformer will accelerate the rate of thermal aging, resulting in a decreased insulation performance and easily causing equipment damage.

Statistics show that in the actual operation of transformers, a turn-to-turn short circuit is one of the most common types of initial faults. Approximately 30% of transformer failures are caused by internal winding short circuits [2,3]. Winding faults usually begin with insulation degradation between two adjacent windings and quickly extend to a large number of windings [4]. In the early stage of transformer winding faults, it usually manifests as a local discharge or overheating in the winding. The heat generated at this stage is naturally convected by the oil to other low-temperature areas, thus avoiding arc generation. As the insulation material further deteriorates between turns, the inter-turn insulation resistance decreases, causing an increase in the leakage current and fault coil current within the windings, leading to localized overheating within the coils. This prevents effective heat dissipation by the transformer oil at the fault points, eventually leading to arcing discharge failures that completely break down the inter-turn insulation formation into turn-to-turn

short-circuit failures [5,6]. Therefore, studying the electrothermal characteristics when winding-to-winding faults occur and preventing their development into serious failures that cause losses is significant to guarantee the secure and steady functioning of power networks [7,8].

The complexity of internal magnetic field distribution within transformers becomes apparent when faults occur, leading to changes in the distribution of leakage magnetic fields. This distribution's spatial arrangement is intricately linked to both winding currents and the position of the faults, showing consistent patterns. Even in cases where the short-circuit ratio is minimal, there remains a notable alteration in the leakage magnetic field. Currently, investigations into the transient behavior analysis of the inter-turn short-circuit faults in transformers primarily emphasize electromagnetic characteristics [7,9], as well as the analysis of faulty winding electromotive force [10,11], etc. Ref. [12] proposed an approach to detect the inter-turn short-circuit faults of distribution transformers utilizing loss fluctuations, enabling real-time monitoring of inter-turn short-circuit faults in windings and alerting to insulation degradation. In addition, Ref. [13] studied the electromagnetic and mechanical characteristics during transformer faults and simulated the transformer's model characteristics. Fault currents, electromagnetic properties, and additional operational parameters were obtained through simulation to study the magnetic field and coil force characteristics during turn-to-turn faults. Ref. [14] conducted a numerical study on turn-to-turn short-circuit (TTSC) faults in rectifier transformers by directly coupling internal finite element (FE) models with external circuit models.

When an internal winding short-circuit fault occurs in a transformer, due to the current amplification of several times to tens of times in the shorted turn, the shorted coil will generate significant heat, causing a significant increase in the local temperature of the winding, which in turn will cause a rise in the oil temperature and the temperature of the tank enclosure [15]. Therefore, obtaining the thermal-flow distribution under inter-turn short-circuit malfunction is highly significant for fault diagnosis. Although the direct measurement method is the most accurate temperature distribution monitoring method, it is difficult to obtain a complete internal distribution due to the high voltage and strong electromagnetic interference inside of the oil-immersed transformers, the harsh environment with full oil immersion, and the existing measuring points that only consider the top-level and bottom-level oil temperatures. Therefore, it is necessary to use a multi-physics field simulation approach to obtain a thermal flow field distribution inside of the operating transformers. In Ref. [16], a two-dimensional model of the winding was created for analyzing the winding temperature and transformer electrical characteristics under faults and combined with electro-thermal characteristics for fault identification. Ref. [8] proposed an inversion calculation method based on forward modeling for inter-turn short-circuit faults by transforming the problem into an optimization problem for the optimal parameters of the internal heat source in transformers. This method can effectively perform an online inversion location calculation for inter-turn short-circuit malfunctions in oil-immersed transformers. Ref. [7] used a finite-element electromagnetic–thermal–fluid method to study early insulation degradation impacts on the internal temperatures of transformers and proposed a decision prediction fault diagnosis method based on online sensors according to the observed results.

This article aims to address the issue of electric–thermal characteristic distribution under winding failure in oil-immersed transformers. By using a coupled field–circuit model to compute the electromagnetic distribution characteristics during winding faults in transformers and obtain the distribution of winding losses, based on this, a thermal–fluid-coupled model is used to analyze the changes in winding temperature distribution after a short-circuit fault occurs between turns. Through the simulation analysis of a 110 kV transformer case, the accuracy of the transformer's electromagnetic–thermal–fluid multiphysics field coupling model has been verified, and, on this basis, we have analyzed its electrical and thermal characteristics under inter-coil short-circuit malfunction.

2. Simulation Model of "Field–Circuit" Coupling for Inter-Turn Faults in Windings, and Calculation of Loss Distribution

2.1. Transformer Three-Dimensional Geometric Model

The oil-immersed transformer model used in this calculation is SFZ-40000 kVA/110 kV(Guizhou Power Grid Co., Ltd., Guiyang, China), which is a three-phase double-winding power transformer with a YNd11 connection group. The winding coils are composed of materials such as conductors, spacers, bracing bars, and insulating paper using a spiral and twisted continuous structure. For the winding radial directions, there is a low-voltage winding, high-voltage winding, and tap-changer winding. When calculating the transformer electromagnetic field, the iron-core stacking structure exerts minimal influence on the magnetic field distribution of the transformer and can be regarded as a whole. Structures like the spacers, bracing bars, and insulating paper have no impact on the electromagnetic field distribution and can be ignored. The installation structure of the winding conductors has a small influence on the overall leakage magnetic field distribution of the windings; it can be replaced by a cylindrical copper material structure as a whole. Structural components such as the oil tanks and clamps have little influence on the magnetic field distribution of the iron core or windings; their impact can be disregarded. Consequently, we set up an ideal calculation domain that enveloped the iron core and windings with rectangular prisms where its border met the magnetic insulation requirements according to the design parameters provided by the transformer manufacturer, as shown in Table 1. The electromagnetic field calculation model of the transformer is shown in Figure 1.

Table 1. Transformer technical parameters and model dimensions.

Parameters	Value	Parameters	Value
Rated capacity	40,000 kVA	Maximum width/thickness of the iron core	590 mm/552 mm
Rated voltage	110 kV ± 8 × 1.25%/10 kV	Height of iron core window	1405 mm
Rated current	209.95 A/2199.43 A	Center distance of iron core	1220 mm
Connection group	YNd11	Length, width, and height of oil tank	4014 mm × 1344 mm × 2745 mm
Number of turns in high-voltage winding	635 turns	Height of high-voltage winding	1220 mm
Number of turns in low-voltage winding	105 turns	Height of low-voltage winding	1220 mm

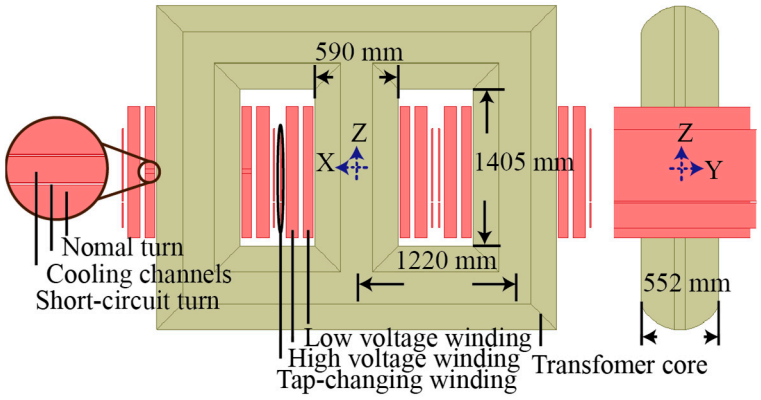


Figure 1. Transformer electromagnetic field calculation model.

2.2. Inter-Turn Short-Circuit Field–Route Coupling Model

Based on Maxwell's equations, the differential equations of the electromagnetic field can be:

$$\nabla \times \nabla \times \mathbf{A} = \mu_0 \mu_r (\mathbf{J} + (\partial \mathbf{D}/\partial t)), \quad (1)$$

where μ_0 denotes the vacuum permeability; μ_r signifies the relative permeability; **J** represents the conduction current density; **D** represents the electric displacement vector; **A** denotes the magnetic vector potential. The initial and subsequent expressions on the right side of Equation (1) signify the conduction current density and displacement current density, correspondingly.

As a consequence of operational conditions and diverse influences, the electrical characteristics of the dielectric materials in power transformers can undergo notable alterations over each transformer's operational lifespan. The decline and aging of transformer insulation are usually caused by the strong electric fields encountered by the transformer, and internal winding faults are caused by the degradation of inter-coil insulation [17]. The electrical properties of the inter-coil insulation material in transformers can be effectively described through a parallel circuit as shown in Figure 2. The insulation thickness between two layers or turns in the windings is very thin, resulting in a very small capacitance value C_{eq} in the equivalent circuit. When the insulation is satisfactory, the resistance Req is high, and the current I_R is minimal. However, as the inter-coil insulation ages and deteriorates, the equivalent resistance gradually diminishes, leading to an equivalent capacitance change. Therefore, there will be a significant increase in the current flowing through the resistor; when an insulation breakdown occurs completely, this resistance will be almost zero.

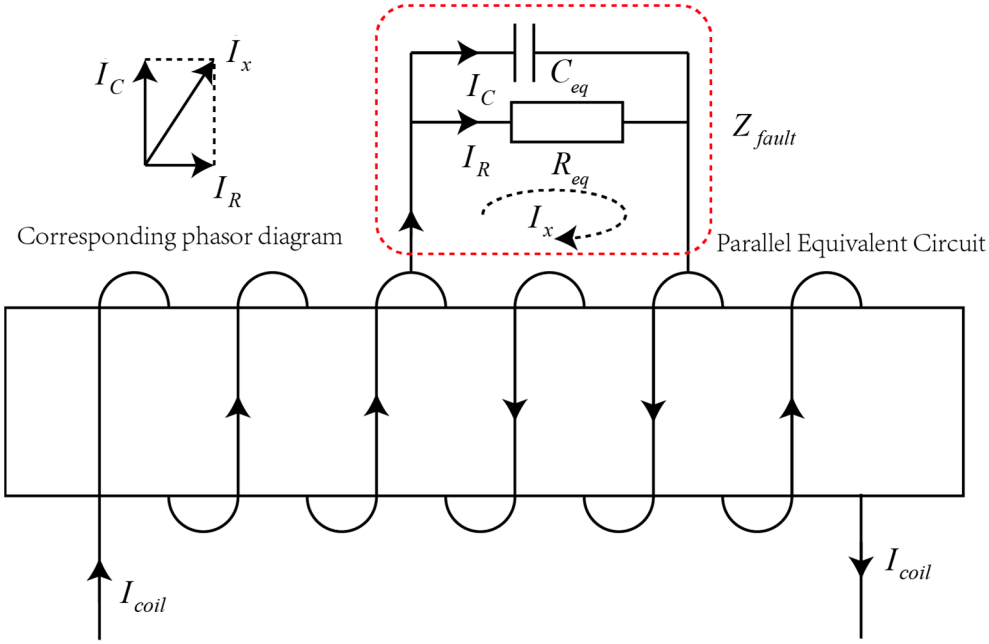


Figure 2. Equivalent winding's turn-to-turn short-circuit model.

The winding coil in the magnetic field is set to be excited by the current, and the circuit elements are introduced according to the short-circuit equivalent circuit of Figure 2, thereby achieving the field–circuit integration of transformer winding short-circuits. This article uses Simulink to build a coupling model of the transformer circuit-magnetic field. The transformer adopts the Y–Δ connection method, as shown in Figure 3. U_{HA}, U_{HB}, and U_{HC} are the three-phase voltages on the high-voltage side; L_{HAO}, L_{HB}, L_{HC}, L_{LA}, L_{LB}, and L_{LC} are the self-inductances of the three-phase windings on the high-voltage side and low-voltage side; R_{HAO}, R_{HB}, R_{HC}, R_{LA}, R_{LB}, and R_{LC} are the DC resistance values of each phase winding on the high-voltage side and low-voltage side; i_{HA}, i_{HB}, i_{HC}, i_{LA}, i_{LB}, and i_{LC} are, respectively, the line current values of each phase winding on the high-voltage side and low-voltage side; i_{LAB}, i_{LBC}, and i_{LCA} are, respectively, the phase current values of each phase winding on the low-voltage side; L_{HAS}, i_{HAS}, and R_{HAS} represent, respectively, the self-inductance value, direct current resistance value, and current for the A-side short-circuited part winding at the low-voltage end; Req is the equivalent short-

circuit resistance value; Z_A, Z_B, and Z_C represent, respectively, the load impedance per phase at the low-voltage end; M_{ASa}, M_{ASAO}, M_{Aoa}, M_{Bb}, and M_{Cc} represent, respectively, the mutual inductance between windings.

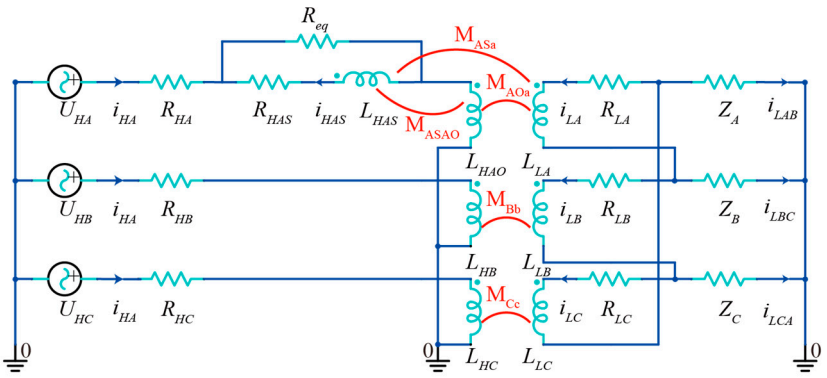


Figure 3. The external circuit model under transformer winding fault.

2.3. Transformer Loss Calculation Method

During the operation of oil-immersed transformers, temperature rise mainly comes from losses generated by windings and iron cores, while stray losses produced by structural components such as clamps are difficult to measure and are generally ignored [18].

According to the IEC 60076-1 standard [19], winding losses are related to the winding current. For faulty windings, winding losses include three parts: non-faulty coil losses, faulty coil losses, and faulty resistance losses. The total load loss under the transformer inter-turn short-circuit malfunction operation may be calculated as follows:

$$P_{coil} = I_n^2 R_n + I_s^2 R_s + P_{se}, \tag{2}$$

where P_{coil} is the total load loss of the coil, W; I_n and I_s represent the current of non-faulty turns and faulty turns, A; R_n and R_s represent the DC resistance of non-faulty turns and faulty turns, Ω; P_{se} is the stray loss of structural components, W. Due to its relatively small proportion, stray losses are generally ignored.

The winding's resistance value correlates linearly with the resistivity of the copper, and there is a linear relationship between the resistivity of the copper and temperature. Consequently, as the temperature rises, the resistivity also increases.

$$\rho_{cu} = \rho_{cu0}(1 + a(T_{cu} - T_{ref})), \tag{3}$$

where the reference resistivity ρ_{cu0} is 1.6679×10^{-8} (Ω·m), the resistivity temperature coefficient a is 3.9×10^{-3} 1/K, and the reference temperature T_{ref} is 293.15 K.

The main loss is the excitation loss generated by the iron core, which can be expressed as follows:

$$P_{total}(f) = P_h + P_c + P_e = K_h f B_m^{\beta} + K_c f^2 B_m^2 + K_e f^{1.5} B_m^{1.5}, \tag{4}$$

where P_{total} represents the iron loss, W/kg; P_h represents the hysteresis loss; P_c represents the eddy current loss; P_e represents the additional loss; f represents the frequency, Hz; k_h, k_c, k_e, and β are undetermined coefficients, obtained through fitting with the loss-curve data. For a given type of silicon steel sheet, k_h, k_c, k_e, and β remain constant and are independent of frequency.

The iron core inside the transformer is made of 30SQG105 silicon steel sheets (Shougang Group, Beijing, China), assembled in a lamination manner with a stacking factor of 0.963. The iron-core loss model coefficient is determined utilizing the BH coefficients furnished by the manufacturer. The calculated loss coefficients are K_h = 37.299, K_c = 0.681, and K_e = 1.374.

3. Transformer Thermal–Fluid Coupling Simulation Model

3.1. Thermal–Fluid Coupling Model

The transformer contains solid components such as iron core, windings, and transformer oil fluid. The main heat transfer methods are solid–solid heat conduction and solid–liquid heat convection, involving the integration principle of temperature field and flow field. The heat generated by the oil-immersed power transformers will eventually be transferred to the surrounding air. The cooling process mainly includes three stages:

1. Heat is conducted from the internal of the iron core and coil to the outer surface;
2. The oil surrounding the iron core and coils is warmed and circulates upward while the cold oil flows downward, forming natural oil convection. When the heated oil reaches the tank wall and cooling fins, heat is transferred to them;
3. Heat from the tank wall and cooling fins is transferred to the ambient air via natural air convection and thermal radiation.

The solution to fluid problems mainly relies on the development of computational fluid dynamics models. The flow dynamics and distribution traits of the oil inside of the transformers follow the fundamental principles of mass preservation, momentum preservation, and energy preservation [20]. The transformer oil behaves as an incompressible Newtonian fluid, and its density does not change over time. The differential form of this fluid can be referenced from [21] as follows:

$$\begin{cases} \nabla \cdot \boldsymbol{V} = 0 \\ \frac{\partial(\rho \boldsymbol{V})}{\partial t} + \nabla \cdot (\rho \boldsymbol{V} \times \boldsymbol{V}) = \rho F - \nabla p + \mu \nabla^2 \boldsymbol{V} \\ \frac{\partial(\rho e)}{\partial t} + \nabla \cdot (\rho e \boldsymbol{V}) = \rho q + \nabla(k \nabla T) - p \nabla \boldsymbol{V} + S \end{cases}, \tag{5}$$

where σ represents the Nabla operator, m^{-1}; V denotes the fluid velocity vector, m/s; ρ represents the fluid density, kg/m^3; F represents the unit mass force of the fluid, m/s^2; p represents the fluid pressure, Pa; μ represents the dynamic viscosity of the fluid, Pa·s; e denotes the internal energy of the fluid, J; q stands for the mass heat source of the fluid, W/kg; k symbolizes the thermal conductivity of the fluid, W/(m·K); S represents the portion of the mechanical energy of the fluid converted into thermal energy due to the combined effect of the oil viscosity and internal heat source of the fluid, J; T indicates the temperature of the transformer oil, K.

3.2. Boundary Conditions

The boundary conditions for the transformer model for the flow field calculation can mainly be divided into three categories. The first category is the flow–solid coupling surface of the iron core, winding, oil tank, and oil. By using the natural circulation of the transformer oil to cool the temperature of the iron core and windings and transferring heat to the surface of the tank body, it can be directly solved through coupling in the ANSYS 2023 R1 FLUENT software system.

The heat conduction process of windings and iron core follows Fourier's principle of heat conduction [22].

$$q_n = -\lambda \frac{\partial T}{\partial n}, \quad n = x, y, z \tag{6}$$

where q_n represents the heat flux; T stands for temperature; λ denotes the thermal conductivity of the windings or iron core.

At the interface between fluid and solid, it is assumed that the fluid adjacent to the wall "film" stagnates in relation to the wall, meaning the relative velocity of the oil flow near the wall is zero. Thus, a no-slip boundary condition is imposed for momentum boundary.

The second type is the contact surface between the transformer box body and its surrounding environment. This boundary includes the top and side surfaces of the box body, mainly through air convection heat dissipation and thermal radiation. In this paper,

the surface of the box body is simplified as a smooth plane, and the surface heat transfer coefficient is derived through solving an empirical equation:

$$h_{con} = \frac{Nu_L \lambda}{L}, \tag{7}$$

$$Nu_L = CRa_L^n, \tag{8}$$

$$Gr_L = \frac{g\beta_{fluid}(T_{sur} - T_{amb})L^3}{{\gamma_{fluid}}^2}, \tag{9}$$

$$Ra_L = Gr_L \mathrm{Pr} = \frac{g\beta_{fluid}(T_{sur} - T_{amb})L^3}{\alpha_t \gamma_{fluid}}, \tag{10}$$

where h_{con} is the convective coefficient of thermal convection; Nu_L represents the Nusselt number; Gr_L signifies the Grashof number; Pr stands for the Prandtl number; β_{fluid} denotes the volume expansion coefficient of the fluid; γ_{fluid} indicates the dynamic viscosity of the fluid in Pa·s; α_t is the thermal diffusivity; Ra_L is the Rayleigh number; T_{sur} is the surface temperature; T_{amb} is the temperature of the ambient. For the laminar flow conditions ($10^4 \leq Ra_L \leq 10^9$), C = 0.59 and n = 1/4. Under a mixture of laminar and turbulent flow conditions ($10^9 \leq Ra_L \leq 10^{13}$), C = 0.10 and n = 1/3.

The indoor transformer is in an environment without solar radiation, so only the radiation of the transformer oil tank to the external environment needs to be taken into account. According to Stefan–Boltzmann law [23], the radiation heat transfer coefficient h_r is:

$$h_r \equiv \varepsilon\sigma(T_a + T_{\mathrm{sur}})\left(T_a^2 + T_{\mathrm{sur}}^2\right) \tag{11}$$

where ε represents the emissivity of the object; σ denotes the Stefan–Boltzmann constant, 5.67×10^{-8} W/(m^2·K^4); T_a indicates the temperature of the object, K.

The third type is the bottom structure. The bottom of the transformer is a grid structure that directly contacts the ground, with a good heat dissipation effect, so it can be set as a temperature boundary condition based on the relationship between the directly measured inlet oil temperature, ambient air temperature, and oil outlet temperature. The transformer radiator usually provides sufficient cooling for the transformer oil, achieving a temperature reduction of about 5–25 K [24]. The outlet is configured with outflow boundary conditions, while the inlet is designated as a velocity inlet.

On top of the electromagnetic field model, add the transformer oil tank structure, ignore the radiator structural components, and retain only the inlet and outlet structures. Additionally, since the transformer structure is basically axially symmetrically distributed, take 1/4 part to form a model for calculating the thermal flow field. The fluid field uses the ANSYS 2023 R1 FLUENT software's mosaic mesh division method and employs the SST k-w model for calculation. This model is not sensitive to the Y+ values of the boundary layers and can appropriately refine the heat transfer solid coupling interface boundary layers; total single mesh count amounts to 511,166 grids.

3.3. Material Parameters

The fuel reservoir is crafted from steel, the coil from copper, and the internal iron core from 30QG105 silicon steel sheets. Typically, alterations in the density, specific heat capacity, and thermal conductivity of solid substances with temperature shifts are minute and can be assumed constant. These material attributes are detailed in Table 2.

Table 2. Thermal parameters of solid materials.

Properties	Copper	30SQG105
Density (kg/m^3)	8900	7650
Specific heat (J/(kg·k))	385	446
Thermal conductivity (W/(m·k))	400	5.22

The transformer winding wires are wrapped layer by layer with an oil-immersed insulation paper, and oil passages are set in the middle of the coil. It is evident from the arrangement of the transformer coil that the fine modeling of the winding wires and oil-immersed insulation paper is very complex, and mesh division is difficult. This article simplifies the structure of the transformer windings based on the thermal parameter equivalence [25]. Using the low-voltage coil as an example to elucidate the winding coil structure and equivalent simplification method, axial consideration includes winding copper wire, insulation paper, and oil passages; radial consideration includes winding copper wire and insulation paper. The thermal conductivity of the materials at 313.15 K is selected for the equivalent calculation: copper has a thermal conductivity of 400, insulation paper has 0.19, and oil has 0.129.

The winding consists of numerous wire loops. Both the axial and radial thermal conductivities (λ_z,λ_r) of the winding are determined using the equation, owing to substantial variations in thermal conductivity between the copper and insulating paper within the winding [26].

$$\lambda_z = \frac{\chi_{z1} + \chi_{z2} + \chi_{z3}}{\frac{\chi_{z1}}{\lambda_{copper}} + \frac{\chi_{z2}}{\lambda_{paper}} + \frac{\chi_{z3}}{\lambda_{oil}}}, \tag{12}$$

$$\lambda_r = \frac{\ln \frac{r_{n+1}}{r_1}}{\sum_{i=1}^{n} \left(\frac{1}{\lambda_n} \ln \frac{r_{n+1}}{r_n} \right)}, \tag{13}$$

where χ_{z1} is the total height of the metal conductor layer in the axial direction of the transformer winding; χ_{z2} is the total height of the oil-immersed insulation paper in the axial direction of the transformer; χ_{z3} is the total height of the oil ducts in the axial direction of the transformer; $r_1, \ldots, r_{n-1}$, and r_n are, respectively, the radial radii of each layer in winding; λ_n is the thermal conductivity of the materials in the radial layers of the winding coils.

The calculation of the equivalent thermal conductivity in each direction of each winding coil is shown as follows in Table 3. The high-voltage winding adopts a twisted continuous coil, while the low-voltage winding adopts a single spiral coil, which is the reason for their different equivalent thermal conductivity.

Table 3. Coil equivalent thermal conductivity.

Thermal Conductivity/(W/(m·K))	Low Voltage	High Voltage	Tap Changing
Axial	0.315	0.494	0.403
Radial	1.4607	0.2266	1.011
Direction of wire winding	400	400	400

Due to the fact that transformer oil serves as the main cooling agent for oil-immersed transformers, its thermodynamic parameters have a significant influence on the thermal distribution within the transformer framework [27]. The thermal–physical parameters of the oil will change with the temperature. In order to ensure fitting accuracy, this paper uses function fitting to describe the variation process of the temperature-dependent thermal–physical properties of the transformer oil [28], as shown in Table 4.

Table 4. Transformer oil physical parameter fitting input formula.

Properties	Fitting Formula
Density $(\mathrm{kg/m^3})$	$\rho_{oil}(T) = -0.6 \times \mathrm{T} + 1057.8$
Thermal conductivity $(\mathrm{W/(m \cdot K)})$	$k_{oil}(T) = -7.101 \times 10^{-5} \times T + 0.1509$
Constant-pressure specific heat $(\mathrm{J/(kg \cdot K)})$	$c_{p,oil}(T) = 0.01T^2 - 3.3463T + 1732.809$
Dynamic viscosity (Pa · s)	$\mu_{oil} = 0.03 \times \left(\frac{T}{293.15}\right)^{-16.7797}$

3.4. Model Validation

This article uses a 40,000 kVA/110 kV three-phase double-winding oil-immersed power transformer for the simulation analysis. Figure 4 shows the overall structure and internal winding structure of the transformer.



(a) Transformer overall structure (b) Transformer winding structure

Figure 4. Transformer casing and winding structure.

To gauge the temperature of the internal coils and the oil temperature within the transformer, 14 optical fibers are used. The fibers are fixed, respectively, in the structural components and inserted into the winding oil passages. To ensure the accuracy of the measurement results, this paper uses the optical fibers produced by the optoelectronics that can operate stably influenced by electromagnetic interference (EMI), radio frequency (RF), and magnetic resonance imaging (MRI) [29]. The fiber-optic temperature sensor has a measurement error of less than 1 K within a temperature range of 233.15 K to 533.15 K, with a diameter smaller than 3 mm, thus it can be securely installed at the position of the winding support bars.

According to the IEC 60076-2:2011 [30], under the condition of an ambient temperature of 299.03 K, a rated load current experiment was conducted on the transformer body. The same ambient temperature and load were used to set the boundary conditions for the simulation model integrating the electromagnetic, thermal, and fluid flow fields of the transformer, and simulation calculations were performed.

Compare the simulated winding temperature, top oil temperature, and oil tank surface temperature with the experimental results to validate the efficiency of the simulation framework. At a temperature of 348.15 K, the high-voltage winding loss is 60648.72 $\mathrm{W/m^3}$, and the loss in the low-voltage coil amounts to 68674.66 $\mathrm{W/m^3}$.

During the experiment, the temperature measurement system collected data on the winding every 5 min. The experimental measurement and simulation calculation values

of the winding temperature are compared in Table 5 below. Observably, the maximum deviation between the simulated winding temperature and the experimental measurement is 3.89 K.

Table 5. Comparison of temperature calculation errors.

Measurement Point	Experimental Measurement Value	Simulated Calculation Value	Error
Low-voltage winding 90% temperature	362.01 K	365.38 K	3.37 K
Low-voltage winding 80% temperature	356.12 K	353.24 K	2.88 K
Low-voltage winding 30% temperature	345.99 K	349.45 K	3.46 K
High-voltage winding 90% temperature	355.20 K	351.31 K	3.88 K
High-voltage winding 80% temperature	347.32 K	349.61 K	2.29 K
High-voltage winding 30% temperature	337.26 K	341.15 K	3.89 K

The distribution of the winding temperatures obtained by the simulation calculation is shown in Figure 5. With an increase in the winding height, the winding temperature gradually rises, but there is a slight decrease at the top. Around the high-voltage windings, the oil decreases in density and rises after being heated. During this rising process, the oil's temperature continues to rise, thus further reducing its heat absorption capacity. When the oil flows to the top of the windings, it enters a radiator for cooling through an outlet. Subsequently, some of the cooled oil returns to bottom of high-voltage windings while another part directly sinks and intersects with the rising hot oil. The flow characteristics of the rising hot oil and sinking cool oil create better heat dissipation conditions at the lower parts of the windings; relatively speaking, the heat dissipation conditions at the upper parts are poorer. This results in a temperature gradient distributed along with the height of the windings. Due to the better heat dissipation conditions, there is a slight decrease in the temperature at the top portion of the windings.

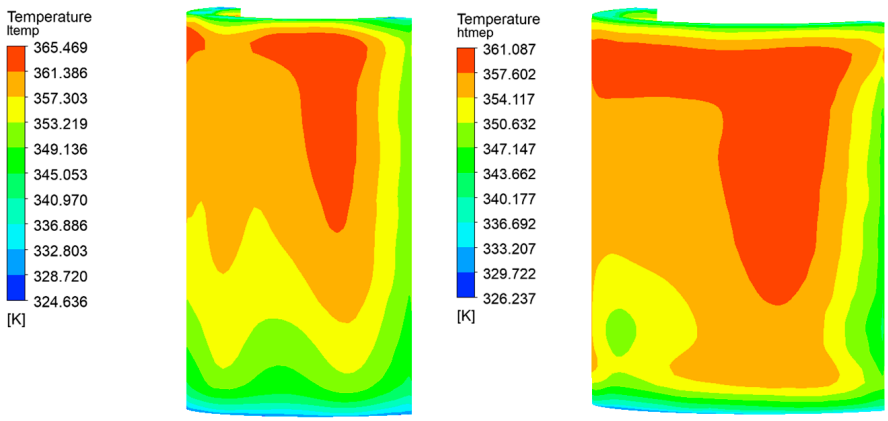


Figure 5. Calculation results of temperature distribution in transformer windings under rated current operation: (**a**) low-voltage winding temperature distribution; (**b**) thermal profile of high-voltage coil.

The temperature distribution across the enclosure surface is illustrated in Figure 6. The differential in the temperature between the top and bottom surfaces of the enclosure is attributed to the thermal convection from the transformer oil flow and the radiator's circulation effect.

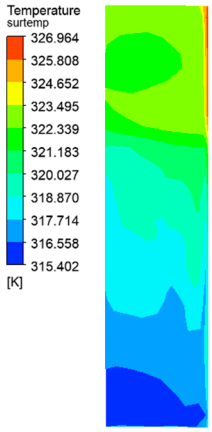


Figure 6. Temperature profile across the tank surface.

4. Analysis of the Thermal Characteristics of the Winding under Inter-Turn Faults in High-Voltage Windings

This section uses a transformer thermal–fluid coupling simulation model to conduct inter-turn fault simulation and analyze the steady-state results of inter-turn faults. The focus is on analyzing the changes in the winding, current, and other electrothermal characteristic parameters before and after the inter-turn faults. During the operation of the transformer, these electrothermal characteristic parameters can be obtained through the current transformers, thermocouples, or online monitoring of the thermocouples. Studying the changes in these electrothermal characteristic parameters can provide new insights for identifying early physical faults in transformers.

4.1. Analysis of the Thermal Characteristics under the Condition of Complete Turn-to-Turn Short-Circuit Faults in Transformers

Supposing the ambient temperature registers at 299.03 K, the low-voltage coil of the transformer bears its rated resistive load, and a turn-to-turn malfunction manifests in the 37th loop within the midpoint of the high-voltage winding, accounting for 1.42% of the total coil turns. The fault turn current changes with the resistance value of the short-circuit fault as shown in Figure 7. This assumes that the inter-turn insulation changes from "good" to 1 Ω at 50 ms, from 1 Ω to 0.1 Ω at 70 ms, from 0.1 Ω to 0.01 Ω at 90 ms, from 0.01 Ω to 0.001 Ω at 110 ms, and from 0.001 Ω to 0.0001 Ω at 130 ms, and a complete short circuit occurs at 150 ms. Based on this, the short-circuit turn current changes with inter-turn insulation and time as shown in Figure 7.

The transformer configuration chosen for this study is Ynd11. When a high-voltage turn-to-turn short circuit emerges during low-load situations, the fault phase current on the high-voltage side undergoes a slight uptick, while the remaining phases exhibit marginal alterations, as depicted in Figure 8. Both the phase current and line current on the low-voltage side witness minimal impact, suggesting that upon detecting a minor turn-to-turn short circuit fault, transformer currents experience negligible shifts, rendering detection arduous and possibly resulting in prolonged operation with faults, thereby jeopardizing the integrity of the transformer equipment, potentially leading to its deterioration or even destruction.

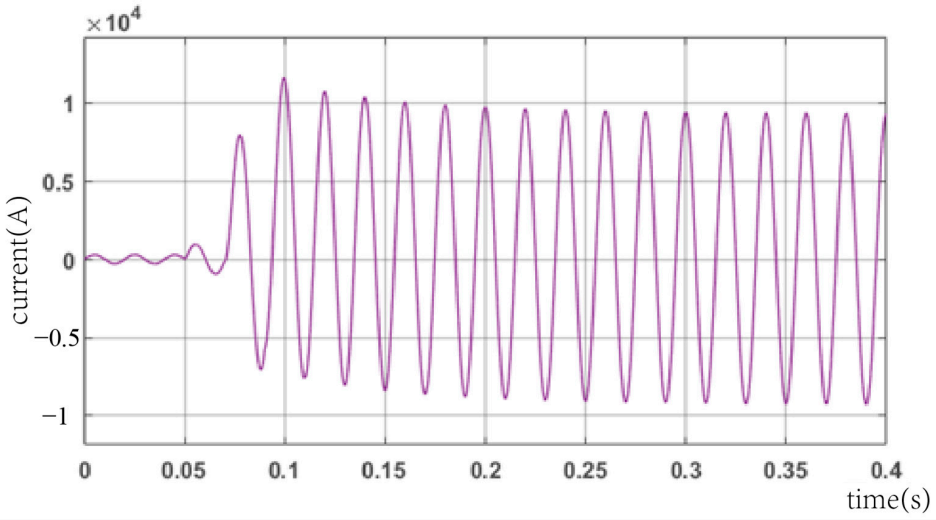


Figure 7. Short-circuit turn current.

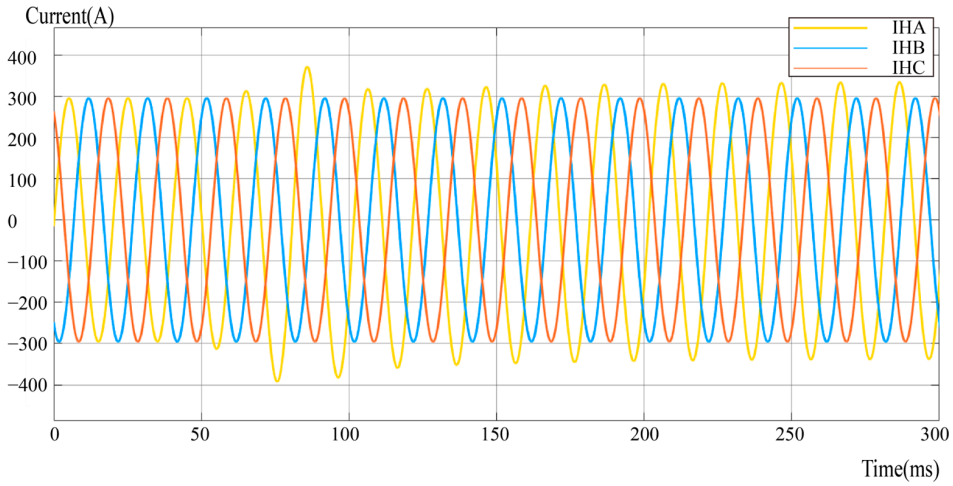


Figure 8. High-voltage side current.

As the time constant of the winding and the temperature rise of the transformer oil far exceed the transformer's period, significant current fluctuations arise within the first two cycles following a turn-to-turn short circuit event. Approximately ten cycles later, the current gradually stabilizes. Consequently, this study opts to utilize the effective current value 2 s post the occurrence of a turn-to-turn short circuit to compute near-steady electromagnetic fields. The effective current values are presented in Table 6.

Table 6. The effective value of current after a malfunction occurs.

	Low-Voltage Current (A)	High-Voltage Current (A)
Phase A	1261.50	237.50
Phase B	1265.96	209.31
Phase C	1266.42	209.38
Short-circuit turn current	/	6576.48

When a turn-to-turn short-circuit fault arises at the midpoint of the high-voltage winding, the temperature alteration in the faulty coil within that layer is particularly pronounced. Figure 9 illustrates the temperature distribution cloud map of the high-voltage winding subsequent to the fault occurrence. As depicted in the diagram, following a turn-to-turn short-circuit fault in the high-voltage winding, the maximum temperature

reaches 394.9 K within 3 s, surpassing the insulation limit of 378.15 K for transformers, which could lead to structural damage to the transformer winding. Furthermore, it attains the temperature limit in 1.7 s, suggesting that a complete winding fault short circuit can cause severe damage to the transformer within an exceedingly brief timeframe. Hence, it is imperative to endeavor to minimize the occurrence of complete winding fault short circuits whenever possible.

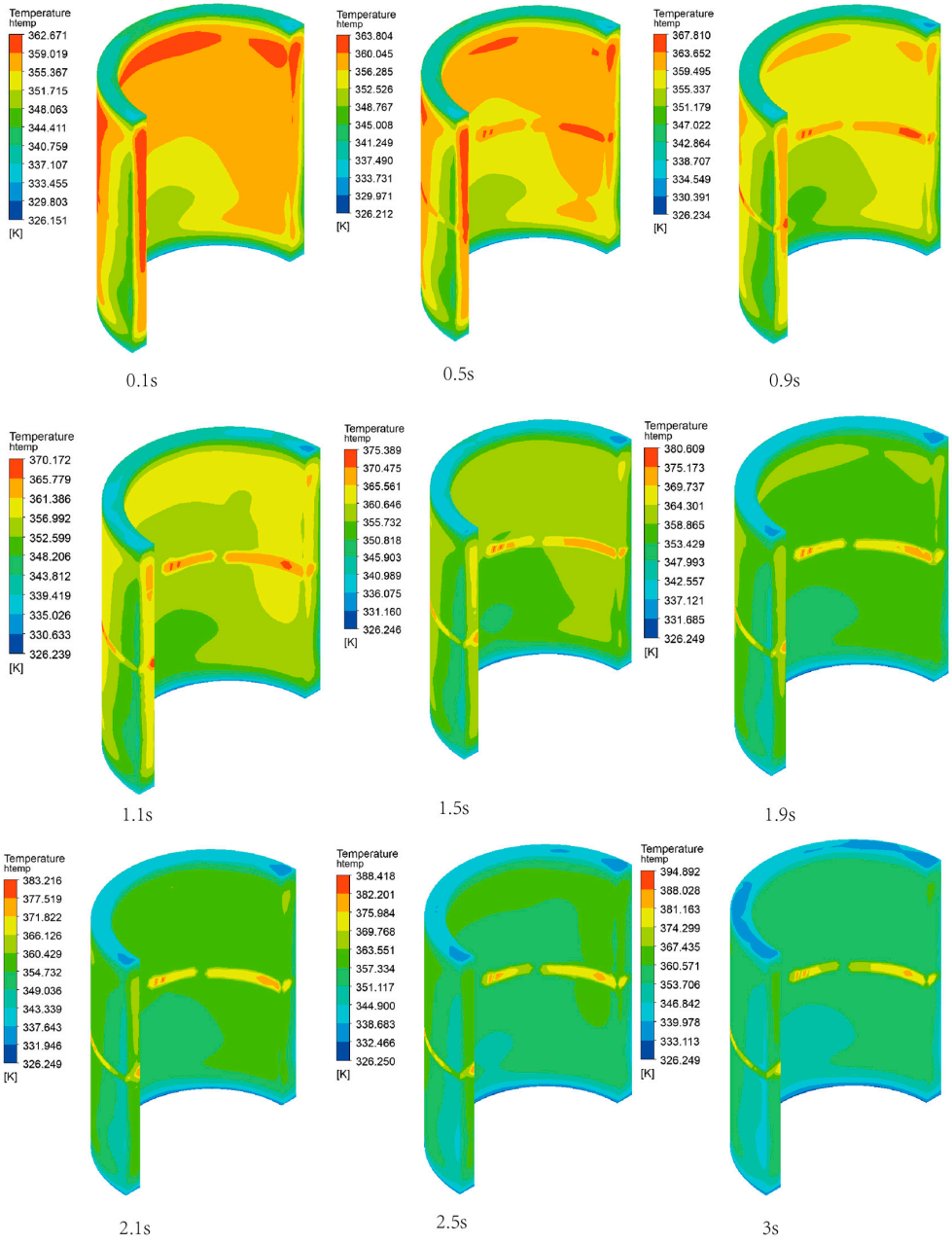


Figure 9. Temperature distribution of high-voltage winding.

4.2. Analysis of the Thermal Characteristics of Inter-Turn Short-Circuit Faults in Transformers under Different Fault Turn Numbers

The quantity of defective coil turns also significantly impacts the electrical heating attributes. Considering the quantities of defective turns as 9, 18, and 27, respectively, which correspond to 1.42%, 2.83%, and 4.25% of the total turns, the computed currents are detailed in Table 7. The temperature distribution of both low-voltage and high-voltage windings following a fault event is illustrated in Figure 10. As depicted in Figure 10, a greater number of faulty turns results in a more pronounced temperature escalation.

Table 7. The effective value of current after a malfunction occurs.

	Low-Voltage Current (A)			High-Voltage Current (A)		
	1.42%	**2.83%**	**4.25%**	**1.42%**	**2.83%**	**4.25%**
Phase A	1261.51	1261.51	1261.51	221.06	256.37	310.04
Phase B	1265.96	1265.96	1265.96	209.31	209.31	209.31
Phase C	1266.42	1266.42	1266.41	209.38	209.38	209.38
Short-circuit turn current		/		664.15	1463.62	2166.68

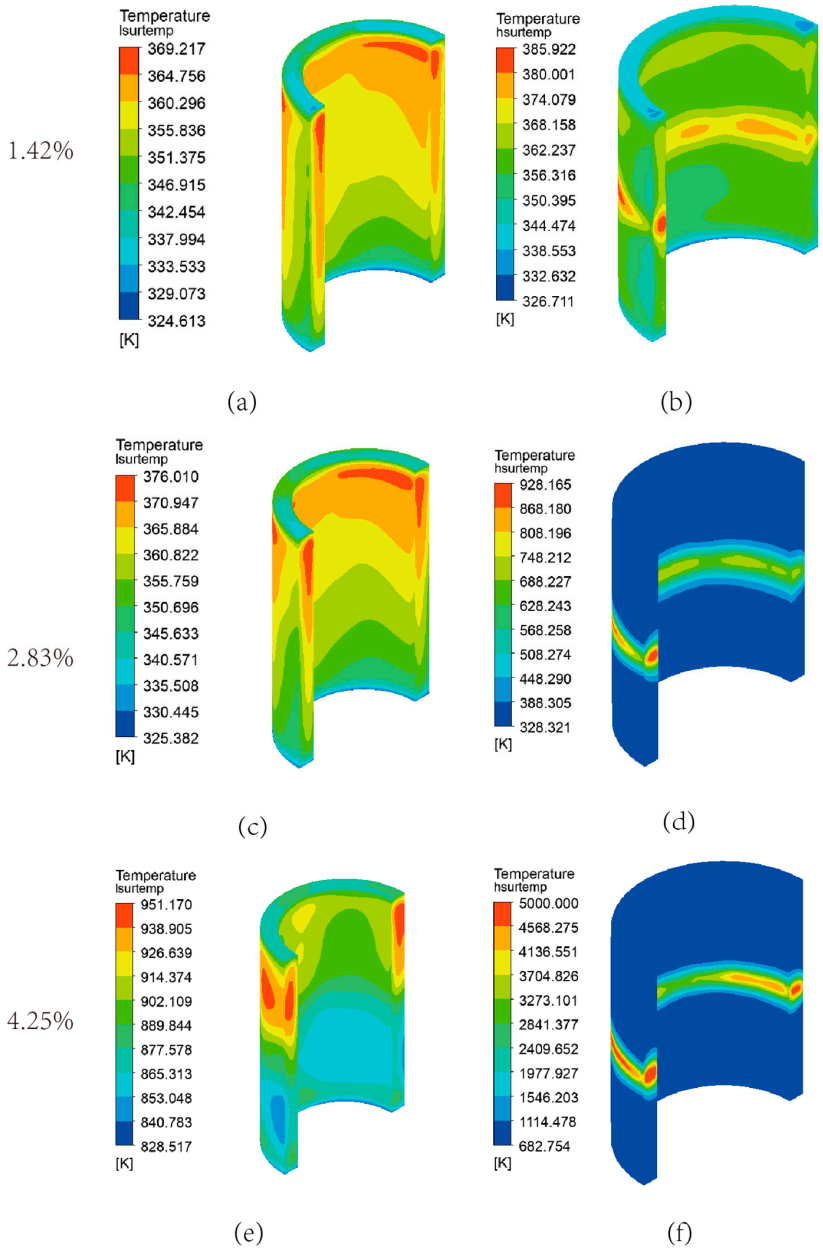


Figure 10. Temperature distribution of windings under different number of faults. (**a**) Temperature distribution of low-voltage winding when the short-circuit turns ratio is 1.42%. (**b**) Temperature distribution of high-voltage winding when the short-circuit turns ratio is 1.42%. (**c**) Temperature distribution of low-voltage winding when the short-circuit turns ratio is 2.83%. (**d**) Temperature distribution of high-voltage winding when the short-circuit turns ratio is 2.83%. (**e**) Temperature distribution of low-voltage winding when the short-circuit turns ratio is 4.25%. (**f**) Temperature distribution of high-voltage winding when the short-circuit turns ratio is 4.25%.

4.3. Analysis of the Thermal Characteristics of Inter-Turn Short-Circuit Faults Occurring in Different Turn-to-Turn Fault Positions of Transformer

Inter-turn faults appearing at various locations within the transformer windings will also have an impact on the temperature distribution of the windings. Inter-turn faults are set to occur at 25%, 50%, and 75% of the high-voltage winding, with a fault resistance set to 1 Ω. The fault location minimally impacts the winding current, as shown in the temperature distribution calculation results in Figure 11.

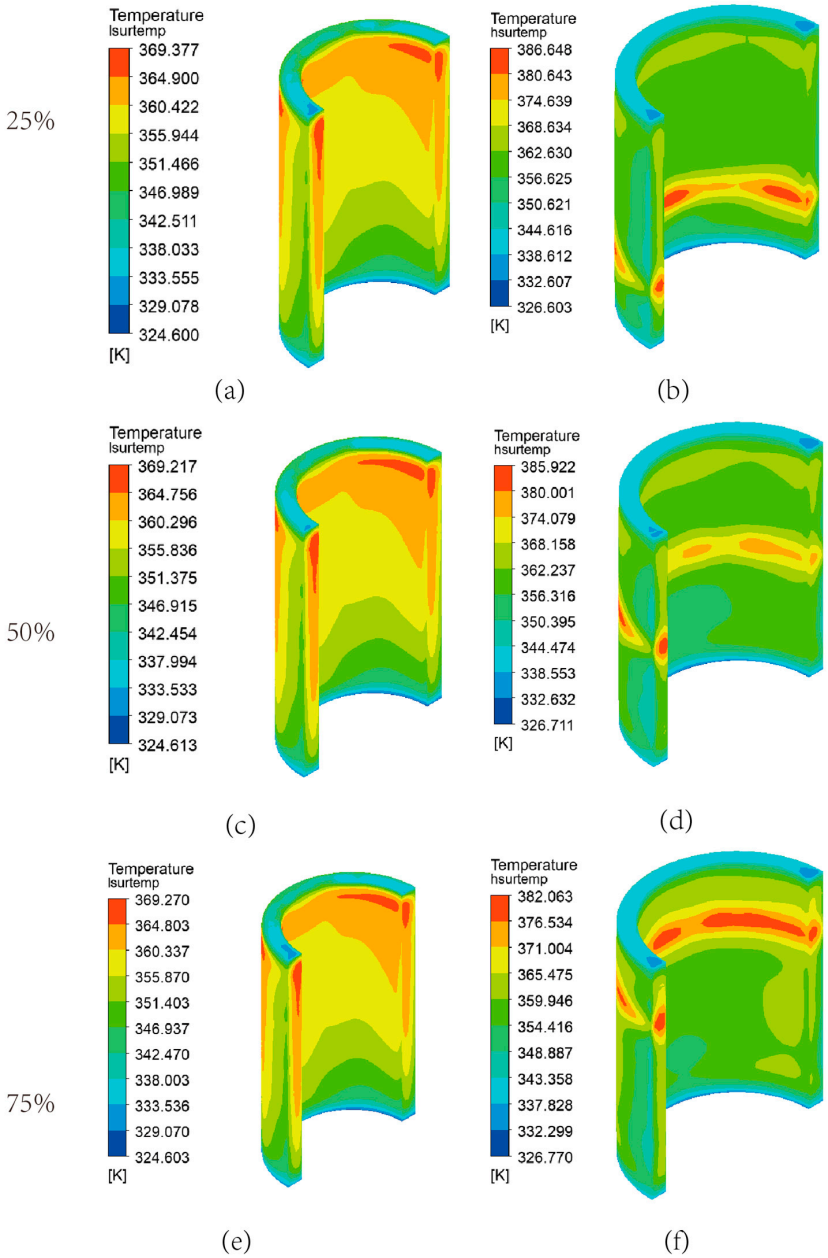


Figure 11. Temperature distribution of windings under different fault locations. (**a**) Low-voltage winding temperature distribution results when a fault occurs at 25% height of the high-voltage winding. (**b**) High-voltage winding temperature distribution results when a fault occurs at 25% height of the high-voltage winding. (**c**) Low-voltage winding temperature distribution results when a fault occurs at 50% height of the high-voltage winding. (**d**) High-voltage winding temperature distribution results when a fault occurs at 50% height of the high-voltage winding. (**e**) Low-voltage winding temperature distribution results when a fault occurs at 75% height of the high-voltage winding. (**f**) High-voltage winding temperature distribution results when a fault occurs at 75% height of the high-voltage.

5. Conclusions

(1) A model for inter-turn faults in oil-immersed transformers was developed, integrating electromagnetic, thermal, and fluid dynamics. This model enables the analysis of the initial electrical and thermal traits of the inter-turn faults. Subsequently, a simulation model for the transformer's thermal–fluid field was constructed. The findings reveal a temperature error of less than 5 K in the simulated winding, validating the efficiency of the established thermal–fluid coupling simulation model for the transformers.

(2) In the case of a complete turn-to-turn fault, due to the star-delta connection method used in the transformers, there is little change in the phase current of the low-voltage windings while the phase current of the high-voltage windings with faults increases significantly, and there is a notable increase in the line current for faulty coils. With a 1.4% complete turn-to-turn fault, the amplitude of the low-voltage winding currents increased by more than 30 times. The fault location has an impact on the temperature distribution of the faulty windings but does not significantly affect the winding currents or maximum temperatures.

(3) The method in this article can analyze the electrical and thermal characteristics of transformer winding faults, providing a simulation dataset for diagnosing inter-turn faults in transformers. Due to the slow thermal time constant inside the transformer, when a minor inter-turn fault occurs in the transformer, it may operate with the fault for a long time until it causes serious damage to the transformer.

Author Contributions: Conceptualization, Y.H. and Z.Z.; data curation, J.X. and H.Z.; formal analysis, H.Z.; funding acquisition, Z.Z.; methodology, Y.H. and Z.Z.; project administration, Z.Z.; resources, Y.Y.; software, Y.H. and H.Z.; supervision, J.X. and Z.D.; validation, Y.H., J.X. and Y.Y.; visualization, Y.Y.; writing—original draft, Y.H.; writing—review and editing, Y.H., Z.Z. and Z.D. All authors have read and agreed to the published version of the manuscript.

Funding: This research and APC was funded by the National Natural Science Foundation of China (grant number: 52077012).

Data Availability Statement: Data are contained within the article.

Conflicts of Interest: Author Jiayi Xiao is employed by the company State Grid Hunan Extra High Voltage Substation Company. Author Hui Zhao is employed by the company Central Southern China Electric Power Design Institute. The remaining authors declare that the research was conducted in the absence of any commercial or financial relationships that could be construed as a potential conflict of interest.

References

1. Kumar, A.; Bhalja, B.R.; Kumbhar, G.B. Approach for Identification of Inter-Turn Fault Location in Transformer Windings Using Sweep Frequency Response Analysis. *IEEE Trans. Power Deliv.* **2022**, *37*, 1539–1548. [CrossRef]
2. Metwally, I.A. Failures, Monitoring and New Trends of Power Transformers. *IEEE Potentials* **2011**, *30*, 36–43. [CrossRef]
3. Barzegaran, M.; Mirzaie, M. Detecting the Position of Winding Short Circuit Faults in Transformer Using High Frequency Analysis. *Eur. J. Sci. Res.* **2008**, *23*, 645–659.
4. Farzin, N.; Vakilian, M.; Hajipour, E. Transformer Turn-to-Turn Fault Protection Based on Fault-Related Incremental Currents. *IEEE Trans. Power Deliv.* **2019**, *34*, 700–709. [CrossRef]
5. Wang, H.; Butler, K.L. Finite Element Analysis of Internal Winding Faults in Distribution Transformers. *IEEE Trans. Power Deliv.* **2001**, *16*, 422–428. [CrossRef]
6. Venikar, P.A.; Ballal, M.S.; Umre, B.S.; Suryawanshi, H.M. A Novel Offline to Online Approach to Detect Transformer Interturn Fault. *IEEE Trans. Power Deliv.* **2016**, *31*, 482–492. [CrossRef]
7. Soleimani, M.; Faiz, J.; Nasab, P.S.; Moallem, M. Temperature Measuring-Based Decision-Making Prognostic Approach in Electric Power Transformers Winding Failures. *IEEE Trans. Instrum. Meas.* **2020**, *69*, 6995–7003. [CrossRef]
8. Chen, S. Study on Fault Diagnosis Approaches for Oil-Immersed Transformer Based on Information Fusion Technology. Master's Thesis, North China Electric Power University (Beijing), Beijing, China, 2017.
9. Hao, Y.; Xian, R.; Hu, Y.; Miao, J.; Guo, Y.; Li, J. Research on Transient Characteristics of Interturn Short Circuit of DryType Transformer Based on Field-Circuit Coupled Finite Element Method. *South. Power Syst. Technol.* **2023**, *17*, 90–98. [CrossRef]
10. Zhang, B.; Xian, R.; Yu, Y.; Xie, T.; Gao, H.; Lei, C. Analysis of Physical Characteristics of Power Transformer Windings Under Inter-Turn Short Circuit Fault. *High Volt. Eng.* **2021**, *47*, 2177–2185. [CrossRef]

11. Yu, C. Evaluation Method of Transformer's Ability to Withstand Short-Circuit Current Based on Finite Element Analysis. Master's Thesis, Xi'an University of Science and Technology, Xi'an, China, 2020.
12. Xian, R.C.; Wang, L.L.; Zhang, B.Q.; Li, J.Y.; Xian, R.M.; Li, J.Q. Identification Method of Interturn Short Circuit Fault for Distribution Transformer Based on Power Loss Variation. *IEEE Trans. Ind. Informat.* **2023**, *20*, 2444–2454. [CrossRef]
13. Zhu, N.; Li, J.; Shao, L.; Liu, H.L.; Ren, L.; Zhu, L.H. Analysis of Interturn Faults on Transformer Based on Electromagnetic-Mechanical Coupling. *Energies* **2023**, *16*, 512. [CrossRef]
14. Yan, C.G.; Zhang, P.; Guo, J.X.; Liu, H.; Yang, H.X.; Zhang, B.H. An Improved Coupled FE–Circuit Model for Turn-to-Turn Short-Circuit Faults Inside Converter Transformers. *IEEE Trans. Magn.* **2023**, *59*, 8400205. [CrossRef]
15. Liu, G.; Rong, S.C.; Wu, W.G.; Wang, X.H.; Li, L. A Two-Dimensional Transient Fluid-Thermal Coupling Method for Temperature Rising Calculation of Transformer Winding Based on Finite Element Method. *AIP Adv.* **2020**, *10*, 035325. [CrossRef]
16. Zhang, L.J.; Sheng, G.H.; Hou, H.J.; Jiang, X.C. Detection Method of Interturn Short-Circuit Faults in Oil-Immersed Transformers Based on Fusion Analysis of Electrothermal Characteristic. *Power Syst. Technol.* **2021**, *45*, 2473–2482. [CrossRef]
17. Wang, H.; Butler, K.L. Modeling transformers with internal incipient faults. *IEEE Trans. Power Deliv.* **2002**, *17*, 500–509. [CrossRef]
18. Chi, C.; Yang, F.; Xu, C.; Cheng, L.; Yang, C. A Multi-Scale Thermal-Fluid Coupling Model for ONAN Transformer Considering Entire Circulating Oil Systems. *Int. J. Electr. Power Energy Syst.* **2022**, *135*, 107614. [CrossRef]
19. *IEC/TC 14 Transformatoren IEC 60076-1:2011*; Power Transformers Part 1: General. The International Electrotechnical Commission: Geneva, Switzerland, 2011.
20. Santisteban, A.; Delgado, F.; Ortiz, A.; Fernandez, I.; Renedo, C.J.; Ortiz, F. Numerical analysis of the hot-spot temperature of a power transformer with alternative dielectric liquids. *IEEE Trans. Dielectr. Electr. Insul.* **2017**, *24*, 3226–3235. [CrossRef]
21. Torriano, F.; Chaaban, M.; Picher, P. Numerical Study of Parameters Affecting the Temperature Distribution in a Disc-Type Transformer Winding. *Appl. Therm. Eng.* **2010**, *30*, 2034–2044. [CrossRef]
22. Yang, S.; Tao, W. *Heat Transfer*; Higher Education Press: Beijing, China, 2006; ISBN 978-7-04-018918-6.
23. Bergman, T.L.; Lavine, A.S.; Incropera, F.P.; DeWitt, D.P. *Fundamentals of Heat and Mass Transfer*, 8th ed.; Wiley: Hoboken, NJ, USA, 2018; ISBN 978-1-119-35388-1.
24. Paramane, S.B.; Van der Veken, W.; Sharma, A. A Coupled Internal–External Flow and Conjugate Heat Transfer Simulations and Experiments on Radiators of a Transformer. *Appl. Therm. Eng.* **2016**, *103*, 961–970. [CrossRef]
25. Deng, Y.; Ruan, J.; Gong, Y.; Daochun, H.; Qingyuan, Z. Three dimensional thermal fluid field simulation of 10kV transformer based on parameter thermal equivalence. *Electr. Power Autom. Equip.* **2021**, *41*, 212–218. [CrossRef]
26. Wang, X. Analysis of Flow-Thermal Coupling of Oil-Immersed Power Transformer Windings Based on Equivalent Thermal Conductivity Method. Master's Thesis, North China Electric Power University, Beijing, China, 2021.
27. Liao, C.B.; Ruan, J.J.; Liu, C.; Wen, W.; Du, Z.Y. 3-D Coupled Electromagnetic-Fluid-Thermal Analysis of Oil-Immersed Triangular Wound Core Transformer. *IEEE Trans. Magn.* **2014**, *50*, 8401904. [CrossRef]
28. Zhang, J.; Li, J.; He, J.; Ma, R. Research on Specific Heat Capacity of Transformer Oil Measured by DSC. *Transformer* **2012**, *49*, 48–50. [CrossRef]
29. Optsensor. Available online: http://www.optsensor.com/product-11994-14338-53712.html (accessed on 1 June 2022).
30. *IEC/TC 14 Transformatoren IEC 60076-2:2011*; Power Transformers Part 2: Temperature Rise for Liquid-Immersed Transformers. The International Electrotechnical Commission: Geneva, Switzerland, 2011.

Disclaimer/Publisher's Note: The statements, opinions and data contained in all publications are solely those of the individual author(s) and contributor(s) and not of MDPI and/or the editor(s). MDPI and/or the editor(s) disclaim responsibility for any injury to people or property resulting from any ideas, methods, instructions or products referred to in the content.